

## Accessing Surface Plasmons with Ni Microarrays for Enhanced IR Absorption by Monolayers

Shaun M. Williams, Amanda D. Stafford, Kenneth R. Rodriguez, Trisha M. Rogers, and James V. Coe\*

Department of Chemistry, The Ohio State University, 100 West 18th Avenue, Columbus, Ohio 43210-1173

Received: April 8, 2003; In Final Form: August 27, 2003

Surface plasmons have been accessed with mid-IR light on Ni microarrays of subwavelength apertures using zeroth-order FTIR transmission spectra. A number of transmission resonances are observed throughout the mid-IR region, which is particularly interesting because nickel's dielectric properties are unfavorable in the visible. On the strongest resonance, these microarrays transmit about 3 times the intensity of light that is directly incident upon the holes (i.e., they exhibit Ebbesen's extraordinary transmission effect). A study is presented of the dispersion and line shape of resonances for a mesh of well-defined geometry (6.5- $\mu\text{m}$ -wide square holes, square lattice with 12.7- $\mu\text{m}$  hole-to-hole spacing, and 5- $\mu\text{m}$  thickness). The dispersion diagram reveals large band gaps (as a fraction of the resonance energy) that are complicated by the lifting of nominally degenerate resonances. The line shape of the most isolated resonance was fit to a damped harmonic oscillator model revealing the complex dielectric parameters including the damping constant. Lifetimes obtained from the damping constants range from 80 to 510 fs and exhibit an exponential dependence on the resonance wavelength. A great enhancement of resonant transmission relative to the fractional open area has also been observed upon stacking two or more meshes on top of each other. The metallic microarray transmission geometry converts the photon energy to surface plasmon polaritons traveling along the metal surface and therefore through coatings, membranes, or monolayers on the mesh. This dramatically changes the path length in absorption experiments from about twice the thickness of the coating (as it is in reflection absorption experiments) to the thickness of the microchannel and more, which could amount in practice to a 1000-fold enhancement in the fraction of light absorbed. These observations suggest opportunities for using these resonances in sensitive detection schemes with vibrational spectroscopies to detect molecular surface species. We show one exciting outcome that involves some unusually large absorbances by 1-dodecanethiolate monolayers on these Ni meshes.

### Introduction

The generation of surface plasmons at metal interfaces is central to a number of new methods for the sensitive detection and assay of molecules, membranes, and nanostructures at interfaces.<sup>1,2</sup> The emerging use of near-field optics to image and investigate structures smaller than the wavelength of light extensively employs surface plasmons. Pohl states<sup>3</sup> that a surface plasmon polariton "may be excited in structures of any size, but excitations in small structures are distinguished by a pronounced resonant character, resulting in a variety of interesting, even spectacular optical phenomena." Surface plasmons (SPs) or surface plasmon polaritons (SPPs) are coherent oscillations of the conducting electrons upon the interaction of light with the conductor surface.<sup>2,3</sup> They are often characterized<sup>4</sup> in terms of dispersion (i.e., the dependence of the SPP resonant energy on the angle of the incident exciting light). Originally, distinctions were intended in the use of the word polariton; however, the terms surface plasmon (SP) and surface plasmon polariton (SPP) seem to be used interchangeably<sup>5</sup> nowadays. The SP has "obtained popularity as the principle in advanced immunosensors, optoelectronic devices, and spectroscopic instruments."<sup>3</sup> The observation of SPs is correlated with nonlinear

optical properties<sup>4,6,7</sup> and suggests opportunities for performing surface-enhanced IR absorption and Raman spectroscopy as well as second harmonic generation spectroscopy at the surface. Furthermore, there now exists a vast body of work using SPs to sensitively detect binding to biological membranes.<sup>8–19</sup> In this work, we investigate the fundamental properties of a microarray structure with the potential to enable the use of SPs to perform sensitive direct infrared absorption analysis. We present a study of the dispersion of the mesh, the effect of stacking several meshes, and the enhancement of the infrared absorption of monolayers on the mesh. From a spectroscopic standpoint, the transmission spectra of the microarray is a highly structured background of light that complicates surface absorption experiments. Of course the optical physics of these resonances is so unusual that it is worthy of study for its own sake. Then we show how the path length can be increased by stacking microarrays, and finally, we show IR absorption spectra of alkanethiol monolayers that exhibit unusually large absorptions.

### Background on Surface Plasmons

A historical perspective on surface plasmons can be gained from Maystre's collection of selected papers,<sup>20</sup> and a good overview is available in Raether's text.<sup>5</sup> Surface plasmon-related

\* Corresponding author. E-mail: coe.1@osu.edu.

phenomena called “Wood’s anomalies” were described as early as 1902 by R. W. Wood.<sup>21</sup> Rapidly changing features in Wood’s spectral anomalies were immediately recognized by Lord Rayleigh<sup>22</sup> as interference effects with evanescent waves that are now known as “Rayleigh edges”, and these features are in fact seen in the present work. Teng and Stern<sup>23</sup> were among the first to measure the dispersion of plasmons that were guided along a metal film’s surface (SPPs) by exciting them with 10-keV electron beams. Cowan and co-workers<sup>24</sup> showed how to make dispersion measurements by varying the angle of incident light on diffraction gratings and described the Lorentzian nature of the surface plasmon resonance as an intermediate state in a photon absorption/re-emission process. One cannot excite a SP directly with a photon because the wave vector of a SP is longer than the wave vector of light of the same energy propagating along the surface (or at any other angle).<sup>5</sup> To excite with light, a device (such as a prism, grating, or subwavelength structure) is required to couple the light and plasmon. Gratings (such as the biperiodic arrays in this work) convert some momentum of incident light into momentum parallel to the surface in units of  $2\pi/L$ , where  $L$  is the grating period. SPs have been typically observed as absorptions in the light reflected from a grating (in contrast to the present transmission studies). Whether in transmission or reflection, the resonances move in characteristic ways as the angle of the incident light is varied.

Many current chemical applications of SPs involve prisms and attenuated total reflection (ATR) coupling. We mention these as examples of the kind of experiments that could be approached with the new, zeroth-order transmission methods discussed in this work. ATR was first demonstrated with visible light by Otto in 1968.<sup>25</sup> In the simpler Kretschmann–Raether<sup>26</sup> ATR configuration, a metallic film of carefully controlled thickness is applied to a prism. Light within the prism is reflected at the metal film with a greater momentum than in air, allowing the momentum of the light to match the SPs at a particular angle. One simply varies the angle of the incident light while monitoring the intensity of the reflected beam. SPs are optimally excited at the angle of minimally reflected light (i.e., a point at which some diffracted light becomes evanescent (remaining on the surface of the metal) where it can match the momentum of SPs). The ATR configuration can be made extremely sensitive<sup>8</sup> to the effective dielectric constant of the metal interface, and it has become the basis of much biosensor work.<sup>9,10</sup> One approach is to self-assemble a lipid bilayer membrane onto the metal film<sup>11</sup> (on the side opposite to the prism). Binding to the membrane causes a change in the angle of minimum reflected intensity as monitored by a laser reflecting off the other side (Biacore commercial instrument). The addition of a dielectric layer<sup>12</sup> provides a refinement (available in Aviv commercial instruments) called plasmon waveguide resonance (PWR) with which a variety of biological systems have been studied.<sup>13–15</sup> Corn and co-workers<sup>16–19</sup> have described variations on these principles, including imaging and the use of FTIR spectrometers for wavelength-based assay. They also describe some advantages of moving from the visible into the near-IR

Most SP resonance studies take place in the visible on silver or gold surfaces. This can be understood by considering the intrinsic limitation on the spectral width of a SP resonance (i.e., the creation of “electron–hole pairs at the Fermi level” by the SP field<sup>5</sup>). This is called “internal damping” and under the ideal condition of no reflection (or 100% transmission in these experiments) is matched by radiation damping. The minimum possible line width (full width at half-maximum, fwhm) is ideally twice the intrinsic damping ( $2\Gamma_i$ ). For a smooth air/metal

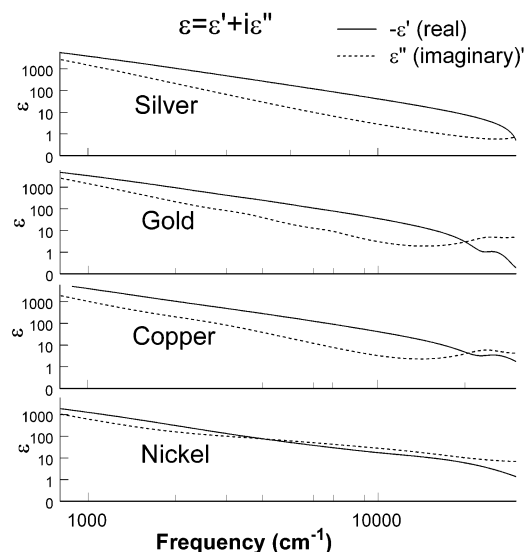


**Figure 1.** Real (solid line) and imaginary (dashed line) components of the dielectric constants of silver, gold, copper, and nickel vs frequency in the infrared and visible regions as calculated with a Lorentz–Drude model.<sup>28</sup> To have long-lived resonances, it is desirable to have the magnitude of the real component greater than the imaginary component, as can be seen with eq 1. Although silver, copper, and gold have good intrinsic properties for SP activity in the visible, nickel becomes good in the infrared only below  $3000\text{ cm}^{-1}$ .

interface, this is

$$2\Gamma_i = 4\pi\tilde{\nu} \left( \frac{\epsilon'_m}{\epsilon'_m + 1} \right)^{3/2} \left( \frac{\epsilon''_m}{2\epsilon'^2_m} \right) \quad (1)$$

where the complex dielectric of the metal is  $\epsilon_m = \epsilon'_m + i\epsilon''_m = (n^2 - k^2) + i(2nk)$  and  $n$  and  $k$  are the often-tabulated real and imaginary parts, respectively, of the complex index of refraction.<sup>27</sup> Radiation damping becomes increasingly important away from the above-mentioned ideal condition, as do other factors such as surface roughness, perforations, or uniformity of the array. Intrinsically, the sharpness of a SP resonance depends on the ratio of the real to the imaginary part of the dielectric constant, such that  $|\epsilon'_m| > \epsilon''_m$  is desired for sharp peaks. Both  $\epsilon'_m$  and  $\epsilon''_m$  are plotted for Ag, Au, Cu, and Ni metals in Figure 1 using a Lorentz–Drude model parametrization.<sup>28</sup> The condition for narrow resonances is satisfied by silver and gold throughout the visible and infrared regions; therefore, these are the metals of choice for work in the visible region. Chemically interesting metals such as nickel (as shown in Figure 1) chromium, palladium, platinum, and tungsten satisfy narrow resonance conditions only in the infrared.<sup>28</sup> In this work, we access SPs simply by recording zeroth-order transmission spectra in an FTIR spectrometer following the nanoarray work of Ebbesen and co-workers in the visible.<sup>29–37</sup> A number of alternative metals and vibrational spectroscopies become available as these methods are pushed into the infrared. We demonstrate these possibilities by accessing SPs on Ni throughout the mid-IR region including a large portion of the range associated with the fundamental vibrations of molecules. By virtue of eq 1 and the dielectric properties of Figure 1, the intrinsic widths of SP resonances generally get narrower as one moves into the IR. The dielectric function for silver in the visible at  $\sim 488\text{ nm}$  ( $\epsilon_m = -7 + i0.7$ ) corresponds to an intrinsic fwhm of  $\sim 2300\text{ cm}^{-1}$ . Silver in the near-IR at  $1.35\text{ }\mu\text{m}$  ( $\epsilon_m = -67 + i6.6$ ) corresponds to an intrinsic fwhm of  $70\text{ cm}^{-1}$ . However, nickel at  $14.3\text{ }\mu\text{m}$  ( $\epsilon_m = -2331 + i1437$ ) corresponds to a

minimum intrinsic fwhm of  $1.2 \text{ cm}^{-1}$ . In fact, Sambles and co-workers<sup>4,38,39</sup> have seen very narrow SP resonances in the ATR configuration with Ni, Pd, Pt, and W at a laser wavelength of  $3.391 \mu\text{m}$ . By working in the mid-IR, we are better able to characterize the dispersion properties and lifetimes of these resonances. These results will provide useful information to those who model, elucidate the coupling mechanisms, and/or adapt such phenomena.

### Extraordinary Optical Transmission of Subwavelength Hole Arrays

The extensively cited work of Ebbesen and co-workers<sup>30</sup> in 1998 on the extraordinary transmission of nanochannel arrays offers a new method of accessing SPs. They fabricated square arrays of cylindrical holes in metallic films (for example, 150-nm-diameter holes, 900-nm hole-to-hole spacing, and 200-nm thickness of silver) and reported unexpectedly large resonant transmissions in the visible and near-IR regions. These films are optically thick (no transmission through the metal) and transmit only by virtue of the perforations.<sup>31</sup> The transmission maximum at  $1.370 \mu\text{m}$  for the film mentioned above is twice the fraction of the open-hole surface area, occurs at a wavelength nearly 10 times the diameter of an individual hole, which is well beyond the waveguide cutoff,<sup>40</sup> and is 1000 times greater (on a per hole basis) than the transmission expected for a single, isolated hole.<sup>30,41–43</sup> Ebbesen's extraordinary transmission effect is attributed<sup>29–31,33–35,37</sup> to an excitation of SPs by incident light that scatters, tunnels, or otherwise propagates through the holes (in a manner currently being elucidated<sup>43</sup>) to SPs on the other side, which can re-emit photons. Some features of the spectra of mesh arrays could be modeled with an array of sources, but it would be very difficult to explain the enhancement of transmission over the amount of light incident directly upon holes without SPs. The evidence for SPs includes (1) the absence of resonant transmissions when germanium is substituted for metal (i.e., a metal is necessary), (2) the much narrower resonances with silver than with chromium<sup>31</sup> because in the near-IR chromium no longer has  $|\epsilon'_m| > \epsilon''_m$  (i.e., the resonance widths are behaving as SPs line widths), (3) the weak transmission of Ni mesh in the visible<sup>33</sup> is enhanced by a very thin coating of Ag, and (4) the angular dependence (dispersion) of transmission spectra (i.e., the way that peaks split and move as a function of the angle of incidence) is roughly described by the behavior of SPs in reflection gratings if an allowance is made for the biperiodicity of the square arrays.<sup>29</sup> It has been suggested that the SPs are acting like mirrors of a Fabry–Perot etalon,<sup>34</sup> trapping photons within the cavity for the femtosecond lifetime of the mirrors, which is long enough for a number of passes to occur. When the film thickness is about the same size as the hole width, coupling between the front and back surfaces occurs, lifting degeneracies while shifting and broadening resonances.<sup>43</sup> Considering the enhanced surface electric fields of SPs and the cavity multipassing effects, there is great scientific and technological potential in the application of metallic subwavelength hole arrays for the sensitive detection of molecules within the holes. There is a need to understand SPs coupling mechanisms better in perforated metal films from both experimental and theoretical perspectives.

The transmission band-pass behavior of biperiodic arrays is a well-known phenomenon<sup>44–48</sup> in the microwave and far-IR regions where the metals can be considered to be perfect conductors. The phenomena of primary interest in this work relate to the complex or absorbing behaviors of real metals that allow SP states to exist and manifest unusual optical properties.

For instance, when the fractional transmission is greater than the fractional open area, then some light is being transmitted through holes even though it is not directly incident upon the hole. The SP-like dispersion behavior is perhaps the strongest evidence for SPs in Ebbesen's work. The unusual dispersion behavior of biperiodic meshes can be roughly predicted<sup>29</sup> by matching the magnitude of light momentum on the grating to the magnitude of SP momentum on the film.<sup>5</sup> Retaining the angular dependence,<sup>29,31</sup> we obtain the resonant wavelength positions as

$$\lambda_{\text{max}} = \frac{L}{i^2 + j^2} (-i \sin \theta + \sqrt{(i^2 + j^2)\epsilon'_{\text{eff}} - j^2 \sin^2 \theta}) \quad (2)$$

where  $L$  is the hole-to-hole spacing (lattice parameter) of the square array,  $\theta$  is the angle of the incident light perpendicular to the film as varied in the direction of the  $i$  index ( $p$  polarization),  $i$  and  $j$  are integer steps along the reciprocal lattice vectors in the horizontal and vertical directions (i.e., indices of the diffraction spots that mix with the zeroth-order transmitted light as they become evanescent with changing wavelength<sup>49</sup>), and  $\epsilon'_{\text{eff}}$  is the real portion of the effective dielectric constant of the perforated film. At  $\theta = 0^\circ$ ,

$$\lambda_{\text{max}} = \frac{L}{\sqrt{(i^2 + j^2)}} n'_{\text{eff}}$$

where  $n'_{\text{eff}} = \sqrt{\epsilon'_{\text{eff}}}$  is the real portion of the effective index of refraction. Consequently,  $n'_{\text{eff}}$  can be estimated by observing the wavelength of resonances at  $\theta = 0^\circ$  as limited by the effect of splitting due to the lifting of degeneracies.<sup>30</sup> The  $(i, j) = (\pm 1, 0)$  or  $(0, \pm 1)$  air/silver resonance in Ebbesen's work<sup>35</sup> occurs at  $1.067L = n'_{\text{eff}}L$ , which implies a greater value of  $n'_{\text{eff}}$  on the perforated metal than on an infinite air/silver interface ( $n'_{\text{eff}} = 1.026$  at  $690 \text{ nm}$  and  $1.010$  at  $1.03 \mu\text{m}$ ).<sup>5,27</sup>

There is currently little theory beyond brute force numerical simulation available to help in interpreting these results. It would clearly be useful to have theoretical predictions of  $n'_{\text{eff}}$  for perforated metal films and/or alternatives to eq 2. Most theoretical work directly invokes SPs, and the dynamic diffraction work of Treacy<sup>50</sup> questions the causal nature of SPs. Computational methods are now available to simulate the transmission spectra of thick biperiodic metallic transmission gratings,<sup>51</sup> but we are aware of only one that calculates transmission versus angle.<sup>50</sup> There are some important 1D studies<sup>52–54</sup> showing the angular effect on the spectra as well as the difference in the dispersion of the waveguide and SP modes,<sup>55–57</sup> but the 2D array behavior is significantly different<sup>51</sup> regarding waveguide modes.

The SP-mediated transmission process has been experimentally shown to be a coherent process<sup>58,59</sup> with a true quantum nature.<sup>58</sup> The transmission process has been investigated with femtosecond pulses by measuring the correlation function between light transmitted through a perforated film and a reference pulse.<sup>59</sup> On the primary resonance, they found a 7-fs transit time through a 300-nm-thick perforated Ag mesh (i.e., a group velocity 7 times slower than the speed of light in vacuum). They also note that a Lorentzian fit to their resonance spectral line shape<sup>59</sup> gives a width that corresponds by the uncertainty principle to the same transit time. The dispersion and resonance dynamics of thick metallic periodic arrays are still challenging problems that could benefit from more incisive experimental data. The lifetime of SPPs will be shown to increase dramatically in the infrared region.

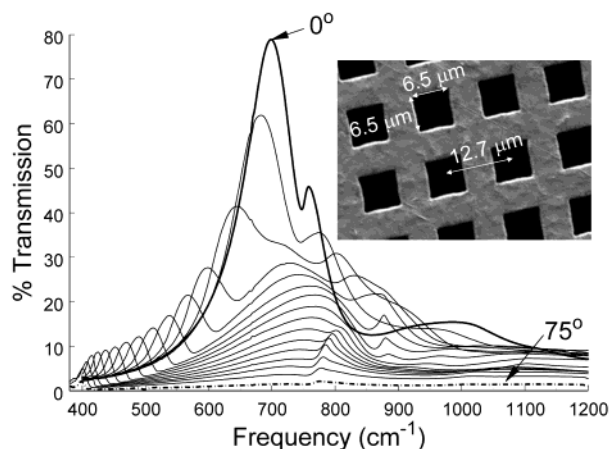


**Figure 2.** Zeroth-order transmission (%T) spectra of Buckbee-Mears Ni mesh vs angle ( $\theta$ ) in the p-polarization active direction. The inset shows a scanning electron microscope image of the Ni mesh, which has 6.5- $\mu\text{m}$ -wide square holes, a square lattice with 12.7- $\mu\text{m}$  hole-to-hole spacing, and 5- $\mu\text{m}$  thickness. The  $\theta = 0^\circ$  trace is shown with a heavier line to aid in distinguishing from the other curves. At  $\theta = 0^\circ$ , one observes a prominent resonance with 77% transmission at 699  $\text{cm}^{-1}$ , which splits into three separate resonances above  $\theta = 10^\circ$ . The lowest-energy set of resonances has been fit to a damped harmonic oscillator model, and the parameters are presented in Table 2.

## Experimental Section

**Zeroth-Order IR Transmission Spectra of a Buckbee-Mears Ni Mesh.** The finest commercially available, biperiodic, metallic mesh (of which we are aware) comes from Buckbee-Mears (278 E. 17th St., St. Paul MN 55101; www.buckbeemears.com). A scanning electron microscope (SEM) image of this mesh is given in Figure 2. It is available only in nickel and has square holes of 6.5- $\mu\text{m}$  width, a square lattice hole-to-hole spacing of 12.7  $\mu\text{m}$ , and a thickness of 5  $\mu\text{m}$ . Although Ni is not useful for generating SPs in the visible regime (see the complex dielectric constant of nickel<sup>28</sup> plotted in Figure 1), it has the right dielectric properties,  $\epsilon''_m < |\epsilon'_m|$ , for wavelengths larger than  $\sim 3 \mu\text{m}$ . The lattice spacing,  $L$  in eq 2, predicts resonances that fall above 3  $\mu\text{m}$  but within the range of a traditional benchtop FTIR instrument. In addition, the wavelength cutoff for a waveguide<sup>40</sup> (an individual microchannel) is nominally twice the hole diameter ( $\sim 13 \mu\text{m}$ ) and does not preclude the observation of any of these resonances (although it could if the holes were much smaller). We have recorded zeroth-order transmission spectra with a Perkin-Elmer Spectra GX FTIR (4- $\text{cm}^{-1}$  resolution, 1- $\text{cm}^{-1}$  steps, 25 scans averaged) at a series of angles from 0 to 75°, in 5° steps, by rotating the mesh about an axis along the  $j$  index, which is aligned with the spectrometer's polarized E field (i.e., in the p polarization or TM active direction, as presented in Figure 2). This set was recorded from 400 to 2000  $\text{cm}^{-1}$  except for the three largest angles that were extended to 350  $\text{cm}^{-1}$  in order to see the lowest-energy resonance at high dispersion. Above 1200  $\text{cm}^{-1}$ , the spectra are relatively flat, ranging from 7 to 5% transmission at 0° owing to an increasing density of increasingly broad and unresolved resonances at higher wavenumbers. We have also recorded a series with the same scanning parameters from 0 to 25.5° in 31 steps, which were used in constructing the dispersion diagram but are not shown in Figure 2.

**Stacking of Meshes.** A simple experiment was performed with this mesh. We clamped and stretched two pieces of Ni mesh on top of each other in rough alignment, which was determined subsequently with an optical microscope. A low-

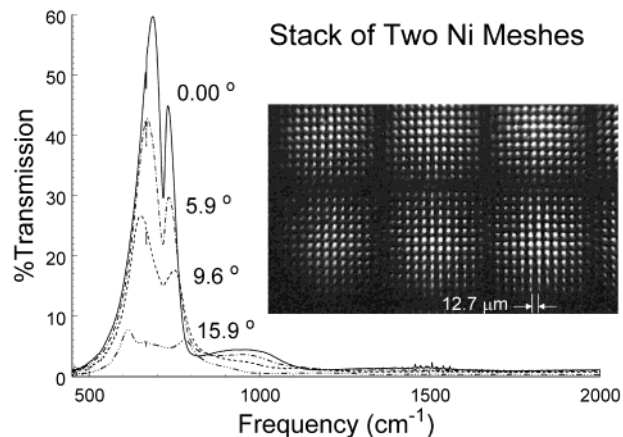


**Figure 3.** Zeroth-order transmission spectrum at  $\theta = 0^\circ$  (solid line) of a stack of two Ni meshes not perfectly aligned. The inset is an optical microscope image of the stack showing a rotation of 2.47° between the two meshes and a 10% open area going straight through both meshes. The stack transmits 60% of the light on resonance even though only 10% is open area. Transmission spectra were recorded vs angle to show the surface plasmon-like dispersion that is similar to that seen with a single mesh (Figure 2). There seems to be less of what might be called “nonmetallic background” with the stack as compared to the single mesh.

magnification, optical microscope image of the two-layer stack was recorded (see inset of Figure 3), which showed a pattern at 305- $\mu\text{m}$  intervals. Analysis revealed that the meshes were rotated from each other by 2.47° and that the fractional open area was 10% (down from the 26% of a single piece of mesh). Transmission spectra were recorded and shown in Figure 3 as a function of angle. Despite the stacking, SP resonances similar to those seen using a single piece of mesh were observed. Finally, we also performed preliminary experiments with four stacked and stretched pieces of mesh in rough alignment (each misaligned by a few degrees from the others). Unfortunately, optical microscope analysis is as not definitive regarding the fractional open area as it is with two pieces; however, we were able to observe 22% transmission on the primary resonance with a crude estimate of 0.5% open area.

**Absorption by Self-Assembled Monolayer on Mesh.** A single piece of Buckbee-Mears Ni mesh was dipped overnight in a solution of 60 mM 1-dodecanethiol in ethanol in order to coat the metal surface with a self-assembled monolayer.<sup>60,61</sup> FTIR zeroth-order transmission spectra at  $\theta = 0^\circ$  were recorded in time. Smooth backgrounds were obtained by fitting a polynomial to points chosen from the low- and high-energy sides of the absorption features. Because there are many broad resonances in this region around 3000  $\text{cm}^{-1}$ , the background is smooth and broad compared to molecular absorptions. Absorption spectra shown in Figure 4 correspond to the negative log of the transmission spectra divided by the corresponding smooth polynomial background. The spectra cover the C–H stretching region for the 1-dodecanethiolate molecule, which consists of a 12-carbon-atom hydrocarbon chain linked to the metal surface by a sulfur atom. There are both methylene ( $\text{CH}_2$ ) and methyl ( $\text{CH}_3$ ) vibrations to be observed in this region.

## Results

**Expectations with Regard to Dispersion.** The relation for the resonant wavelength (eq 2) can be converted to an energy-dispersion relation by substituting  $k_x/(2\pi\nu)$  for  $\sin(\theta)$  and allowing the real portion of the effective dielectric to change

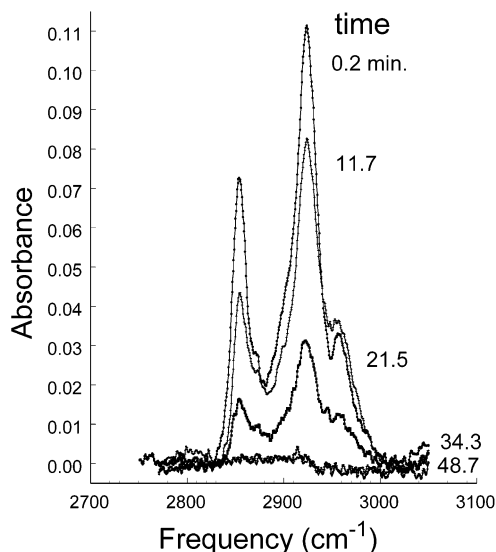


**Figure 4.** Absorption spectra in absolute absorbance units of a 1-dodecanthiolate monolayer on a single piece of Ni mesh in the C–H stretching region. The most intense absorption (asymmetric methylene CH<sub>2</sub> stretch) is more than 100 times more intense than that recorded with reflection absorption infrared spectroscopy. The spectrum decays over the course of half an hour, as is known to happen on nickel. The metallic microarray transmission geometry forces light to go along surfaces (and therefore through coatings, membranes, or monolayers), dramatically changing the path length in absorption experiments.

with wavenumber [ $\epsilon'_m(\tilde{\nu}) = \alpha_0 + \alpha_1\tilde{\nu}^{-1} + \alpha_2\tilde{\nu}^{-2}$ ]:

$$\tilde{\nu}_{ij}(k_x) = -\frac{\alpha_1}{2\alpha_2} + \sqrt{\frac{\alpha_1^2}{4\alpha_0^2} + \frac{1}{\alpha_0}\left(-\alpha_2 + \frac{i^2 + j^2}{L^2} + i\frac{k_x}{\pi L} + \frac{k_x^2}{4\pi^2}\right)} \quad (3)$$

where  $\tilde{\nu}$  is the resonant peak center in wavenumber units. Expanding this to a polynomial in  $k_x$  gives

$$\tilde{\nu}_{ij}(k_x) = \left(-\frac{\alpha_1}{\alpha_0} + \frac{f_{ij}}{2}\right) + \left(\frac{i}{\pi L\alpha_0 f_{ij}}\right)k_x + \left(\frac{1}{4\pi^2\alpha_0 f_{ij}} - \frac{i^2}{L^2\pi^2\alpha_0^2 f_{ij}^3}\right)k_x^2 + O(k^3) \quad (4)$$

with

$$f_{ij} = \sqrt{\frac{\alpha_1^2}{\alpha_0^2} + \frac{4}{\alpha_0}\left(\frac{i^2 + j^2}{L^2} - \alpha_2\right)} \quad (5)$$

If we assume that  $\epsilon'_m$  is constant ( $\alpha_1 = \alpha_2 = 0$  and  $\alpha_0 = \epsilon'_m$ ), then we obtain approximate relations that reveal general trends. The  $(i, j) = (-1, 0)$ ,  $(0, \pm 1)$ , and  $(1, 0)$  resonances would have the same peak center of  $1/(L\sqrt{\alpha_0})$  at  $k_x = 0$ . The  $(-1, 0)$  resonance would have a dispersion slope dominated by the linear term of  $-1/(2\pi\sqrt{\alpha_0})$ , and the  $(1, 0)$  would have a slope of  $+1/(2\pi\sqrt{\alpha_0})$ . The linear term for the  $(0, \pm 1)$  resonance is zero in this approximation, and the quadratic term is  $L/(8\pi^2\sqrt{\alpha_0})$ . At  $700 \text{ cm}^{-1}$ , an infinite air/nickel interface has  $\sqrt{\alpha_0} = 1.00016$ , so this quantity is expected to have a value close to 1.

**Dispersion Diagram.** These IR transmission spectra and their numerical first and second derivatives were simultaneously examined to extract peak centers, Rayleigh edges, and shoulders

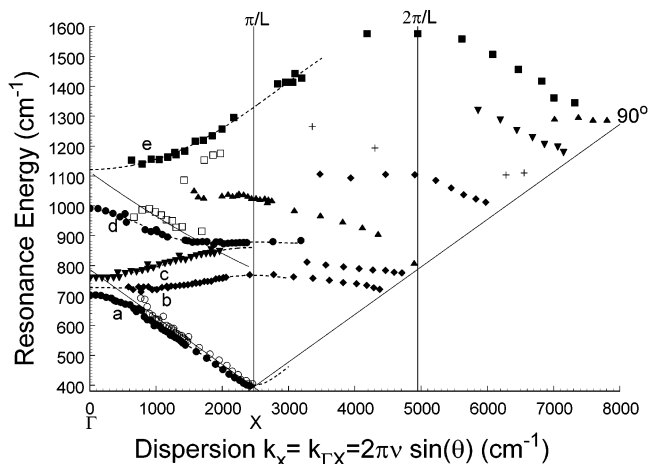


**Figure 5.** Dispersion diagram in the  $\Gamma X$  coordinate for TM polarization of a square lattice for a single piece of Buckbee-Mears Ni mesh. The solid symbols correspond to peak centers of transmission resonances. The open circles correspond to maxima in the first derivative (Rayleigh edges) and show that the resonance set (labeled a) tracks the free-electron curve (solid line) before bending away at low dispersion. The open squares correspond to shoulders indicated by numerical second derivatives. The resonance sets labeled a–e have been fit to smooth polynomial curves (indicated by dashed lines), and the parameters are given in Table 1.

for the construction of a dispersion diagram. These properties are plotted versus dispersion in Figure 5. When modeling such membranes, the incident light direction at  $\theta = 0$  is often taken in the Cartesian  $z$  direction, and the mesh extends in the  $x$  and  $y$  directions, which are respectively taken as aligned with the square lattice along the  $i$  and  $j$  directions of eq 2. Consequently, we use  $k_x$  as the dispersion along the  $i$ -index direction. There are common crystallographic designations associated with the square lattice such that  $k_x$  is often designated as  $k_{\Gamma X}$  in the  $\Gamma X$  direction or  $k_{\Gamma X}$ . The dispersion ( $k_x$  or  $k_{\Gamma X}$ ) is  $2\pi\tilde{\nu} \sin(\theta)$ , where  $\tilde{\nu}$  is taken as the resonance peak center (in  $\text{cm}^{-1}$ ). The angle ( $\theta$ ) is varied in the  $i$ -index direction (rotation about an axis in the  $j$ -index direction) with the orientation of the spectrometer's E field along the  $j$ -index direction (TM or p polarization). The filled symbols in Figure 5 correspond to peak centers, and the open squares correspond to shoulders found with second derivatives. The open circles associated with the lowest-energy resonance (set labeled a in Figure 5) are maxima in the first derivative (i.e., Rayleigh edges). When the peak is sufficiently far away from its closest neighbor, these points fall directly on the free-electron curve, which is drawn as a solid line with a slope of  $-1/2\pi$  and an intercept of  $1/L$  or  $787.4 \text{ cm}^{-1}$ . The band gap can be characterized by the deviation of the peak centers from this line at  $k_{\Gamma X} = 0$  and  $\pi/L$  and the  $\Gamma X$  component of effective electron mass from the curvature of the peak centers at  $k_{\Gamma X} = 0$  and  $\pi/L$ . The ability to detect resonances at angles up to  $75^\circ$  produces data impressively close to the  $90^\circ$  limit, which is shown as a light curve labeled  $90^\circ$  in Figure 5. The high range of accessible angles also enabled the lowest-energy resonance to be sufficiently isolated that it could be fit to a damped harmonic oscillator model revealing lifetimes. These efforts are described in later part of the Results section. Five sets of resonances at low dispersion have been labeled a–e in Figure 5. In the next section, we assign these sets of resonances.

**Assigning Resonance Sets.** Resonances can be attributed to diffraction spots as they become evanescent with changing spectral frequency,<sup>49</sup> so the indices  $(i, j)$  of eq 2 for integral spots along the reciprocal lattice vectors also label diffraction spots. At  $0^\circ$ , the four closest diffraction spots to the center

**TABLE 1: Fits of the Peak Centers of Resonance Sets a–e of Figure 5 to  $\sum_{m=0}^{m_{\max}} \gamma_m \cos(k_x L m)^a$** 

label	assignment	$\gamma_0$ (cm <sup>-1</sup> )	$\gamma_1$ (cm <sup>-1</sup> )	$\gamma_2$ (cm <sup>-1</sup> )	$\gamma_3$ (cm <sup>-1</sup> )	$\gamma_4$ (cm <sup>-1</sup> )	$\gamma_5$ (cm <sup>-1</sup> )	std dev (cm <sup>-1</sup> )
a	(-1, 0)	564.2(6)	140.5(9)	-8.0(8)	8.7(9)	-5.7(9)	1.0(8)	4
b	(0, $\pm 1$ ) <sub>low</sub>	739.9(15)	-20.6(22)	7.2(22)				7
c	(0, $\pm 1$ ) <sub>high</sub>	810.4(11)	-50.4(16)					6
d	(-1, $\pm 1$ )	914.0(10)	54.4(13)	19.6(14)				5
e <sup>b</sup>	(1, $\pm 1$ )	1349(6)	-247(10)	20(9)				11

<sup>a</sup> Errors are estimated standard deviations and are given in parentheses corresponding to the least significant digits. The last column gives the estimated standard deviation of the fit. <sup>b</sup> This set was fit to a polynomial in  $\cos(k_x L m/2)$  rather than  $\cos(k_x L m)$ .

[(1, 0), (0, 1), (-1, 0), and (0, -1)] are symmetric about the undeflected center spot. They are nominally degenerate and become evanescent at the same frequency of  $\sim 700$  cm<sup>-1</sup> producing the prominent resonance. This feature reveals two peaks at  $\theta = 0^\circ$ , so we know that the degeneracy is lifted. Because the (0,  $\pm 1$ ) diffraction spots are not displaced by the change of angle in the  $i$ -index direction ( $k_{\Gamma X}$  direction), they will not separate, and the feature can be expected to break into three distinct peaks with increasing dispersion (i.e., the (-1, 0), (0,  $\pm 1$ ), and (1, 0) resonances). At  $\sim 10^\circ$ , the feature does break into three distinct peaks, but care must be exercised on the basis of the expectations of the preceding section. The lowest-energy resonance set labeled a in Figure 5 is easily assigned to the (-1, 0) resonance as it approaches the free-electron curve (solid line in Figure 5 with a slope of  $-1/(2\pi)$  and an intercept of  $1/L$ ). Apparently,  $\sqrt{\alpha_0} = \epsilon'_{\text{eff}}$  has a value close to 1, not unlike SPs at a nonperforated air/nickel interface in the IR. The set of resonances labeled b in Figure 5 start at  $k_x = 0$  near the (-1, 0) set with an initially flat trend that increases with a fitted term of  $(1.0 \times 10^{-5} \text{ cm})k_x^2$ . This compares reasonably well to  $L/(8\pi^2) = 1.6 \times 10^{-5} \text{ cm}$ , so this set is assigned as the (0,  $\pm 1$ ) resonance (or at least a component of that resonance). The set of resonances labeled c obtains (away from the band gap) a linear term of  $\sim 0.054k_x$ . This is less than  $1/3$  of the slope expected for the (1, 0) resonance ( $+1/(2\pi) = 0.159$ ). Noting that the (0,  $\pm 1$ ) resonance is doubly degenerate, we hypothesize that set c is the higher-energy member of a splitting of the (0,  $\pm 1$ ) resonance. This interpretation leads to the conclusion that the (1, 0) resonance is not observed. Darmanyan and Zatz<sup>62</sup> have shown that not all SPP states can couple to the incident radiation. Although they employed a harmonic model of the perforated surface, they found that the wave function of the upper state in the  $k_{\Gamma X} = 0$  band gaps of a metallic square lattice array was real (i.e., it had no imaginary part and no damping). A state with an infinite lifetime cannot participate in transmission and will not be observed.

The second resonance at  $0^\circ$  and  $\sim 1000$  cm<sup>-1</sup> is attributed to the nominally degenerate (1, 1), (-1, 1), (1, -1), and (-1, -1) resonance peaks. Angle tuning in the  $i$ -index (p-polarization active) direction breaks these into two separate peaks [(-1,  $\pm 1$ ) and (1,  $\pm 1$ )]. The set labeled d in Figure 5 is assigned to the (-1,  $\pm 1$ ) resonance, and the set labeled e is assigned to the (1,  $\pm 1$ ). The (-1,  $\pm 1$ ) collides with the set labeled c within the first Brillouin zone. The solid curve drawn near these peaks is derived from eq 4 with  $i = -1, j = \pm 1, \alpha_2 = \alpha_1 = 0$ , and  $\sqrt{\alpha_0} = 1$ . There are shoulders in the vicinity of the free-electron curve for this resonance set. Again, there is a significant lifting of the degeneracy at  $0^\circ$ .

**Band Gaps and Effective Electron Masses.** The relations in eqs 3–5 do not model the bending of the resonant energy levels as they approach free-electron curve crossings producing band gaps. We have fit the resonant peak centers to a polynomial

in the harmonics of a cosine function of the first Brillouin zone:

$$\tilde{\nu}_{i,j}(k_x) = \sum_{m=0}^{m_{\max}} \gamma_m \cos(k_x L m) \quad (6)$$

The fit coefficients,  $\gamma_m$ , are given in Table 1 for the sets of resonances (a–e in Figure 5). Note that the e set was better fit to a polynomial in  $\cos(k_x L m/2)$ . From these fits, many properties of interest can be determined.

The a or (-1, 0) set has a fitted value of 701 cm<sup>-1</sup> at  $k_x = 0$ , which is 87 cm<sup>-1</sup> below the free-electron curve. We take this as our best estimate of the band gap. Note that this is about 11% of the free-electron band center, which is fairly large,<sup>63</sup> like the meshes of Ebbesen and co-workers.<sup>43</sup> The second derivative at  $k_x = 0$  (which is reciprocally related to the  $\Gamma X$  component of the effective electron mass of the SPP) is  $-1.9 \times 10^{-4} \text{ cm}$ . This is smaller than the second derivative at  $k_x = \pi/L$ , which is  $5.9 \times 10^{-4} \text{ cm}$ . Consequently, the band gap at  $k_x = \pi/L$  is considerably narrower than the one at  $k_x = 0$ .

The ( $\pm 1, \pm 1$ ) feature (sets d and e) also belies a large band gap. The d set has a value of 988 cm<sup>-1</sup> at  $k_x = 0$  that falls 126 cm<sup>-1</sup> below the free-electron curve, which we take as an estimate of the band gap. Again, this is 11% of the free-electron band center, which is large for this property. The second derivative at  $k_x = 0$  of the (-1,  $\pm 1$ ) set is  $-2.1 \times 10^{-4} \text{ cm}$ , which is similar to that of the (-1, 0) set.

**Damped Harmonic Oscillator Fit of the (-1, 0) Resonance Set.** An inspection of Figure 2 reveals an asymmetric line shape for the (-1, 0) resonance set that gets narrower as the resonance shifts to lower energies. To extract lifetimes, we fit this set of resonances to a damped harmonic oscillator model that has been applied to the lattice vibrations of crystals.<sup>64</sup> At  $10^\circ$  and above, the (-1, 0) set was found to be sufficiently isolated from other resonances to be fit. The complex dielectric was taken as

$$\epsilon(\tilde{\nu}) = \epsilon_\infty + \frac{(\epsilon_0 - \epsilon_\infty)\nu_t^2}{(\nu_t^2 - \tilde{\nu}^2) - i\gamma\tilde{\nu}} \quad (7)$$

$\gamma$  is the damping constant,  $\nu_t$  is the transition frequency,  $\epsilon_\infty$  is the high-frequency value, and  $\epsilon_0$  is the low-frequency value, where  $\epsilon_0 - \epsilon_\infty$  is sometimes taken as the line strength. Whereas otherwise transparent crystals absorb and reflect on resonance, our mesh transmits; therefore, we take the reflectivity as 1 minus the reflectivity of a crystal with a lattice vibration, namely

$$R(\tilde{\nu}) = 1 - \left( \frac{1 - \sqrt{\epsilon(\tilde{\nu})}}{1 + \sqrt{\epsilon(\tilde{\nu})}} \right) \left( \frac{1 - \sqrt{\epsilon(\tilde{\nu})}}{1 + \sqrt{\epsilon(\tilde{\nu})}} \right)^* \quad (8)$$

**TABLE 2: Damped Harmonic Oscillator Fit Parameters for the  $(-1, 0)$  Resonance at Different Angles<sup>a</sup>**

$\theta$ (deg)	$\nu_i$ (cm <sup>-1</sup> )	peak center (cm <sup>-1</sup> )	$\gamma$ (cm <sup>-1</sup> )	$\epsilon_0$	$\epsilon_\infty$	$h$ (cm)	std dev (%T)
10°	596.96(14)	646	43.52(11)	1.7321(6)	1.3453(5)	0	0.5
15	567.98(7)	599	34.17(6)	1.7210(3)	1.4200(3)	0	0.25
20	533.46(6)	567	30.58(5)	1.5296(3)	1.2431(3)	$1.909(12) \times 10^{-5}$	0.21
25	506.10(6)	538	26.90(4)	1.6329(3)	1.3360(3)	$4.778(17) \times 10^{-5}$	0.15
30	476.92(8)	512	23.87(5)	1.4428(4)	1.1728(3)	$9.72(4) \times 10^{-5}$	0.20
35	465.40(18)	490	19.82(11)	1.2266(7)	1.0611(6)	$8.9(12) \times 10^{-6}$	0.4
40	450.19(16)	470	17.93(10)	1.2723(6)	1.1181(5)	$8.63(11) \times 10^{-5}$	0.4
45	434.88(13)	452	16.33(8)	1.2968(5)	1.1483(4)	$9.49(11) \times 10^{-5}$	0.3
50	426.94(13)	437	14.37(8)	1.3505(5)	1.2373(4)	$5.09(9) \times 10^{-5}$	0.28
55	415.88(7)	425	12.28(5)	1.4211(3)	1.3106(3)	$6.20(6) \times 10^{-5}$	0.17
60	406.92(9)	416	10.96(6)	1.4571(4)	1.3590(3)	$6.19(9) \times 10^{-5}$	0.20
65	400.85(8)	407	11.56(6)	1.4131(3)	1.3245(3)	$5.26(8) \times 10^{-5}$	0.16
70	396.49(7)	401	10.43(5)	1.3962(3)	1.3284(3)	$4.80(8) \times 10^{-5}$	0.11
75	395.07(15)	398	7.99(9)	1.3897(5)	1.3349(4)	$1.92(4) \times 10^{-6}$	0.10

<sup>a</sup> The standard deviations of the parameters are given in parentheses as the least significant digits in the value. The peak centers have been listed for comparison to  $\nu_i$ . The last column is the standard deviation of the fit. The damping constants are the full-width-at-half-maximum of the imaginary part (absorption part) of the dielectric constant, which has a Lorentzian form and can yield lifetimes. Representative fits are given in Figure 6.

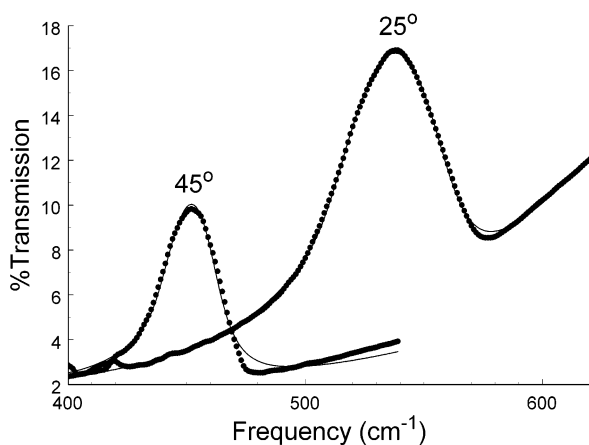


**Figure 6.** Typical fits with a damped harmonic oscillator model of the  $(-1, 0)$  transmission resonances of Buckbee-Mears Ni mesh at  $\theta = 25$  and  $45^\circ$ . Damping parameters were used to obtain lifetimes of the resonances as displayed in Figure 7.

The transmission was modeled with

$$T(\tilde{\nu}) = \frac{(1 - R(\tilde{\nu}))^2 e^{-4\pi\tilde{\nu}Im\{\sqrt{\epsilon(\tilde{\nu})}\}h}}{1 - R(\tilde{\nu})^2 e^{-8\pi\tilde{\nu}Im\{\sqrt{\epsilon(\tilde{\nu})}\}h}} \quad (9)$$

where  $h$  is the effective thickness of the perforated membrane (not the physical thickness). These equations were first used to simulate the background due to the neighboring resonance, and then a nonlinear least-squares fit was performed to find the best-fit values of  $\gamma$ ,  $\nu_i$ ,  $\epsilon_\infty$ ,  $\epsilon_0$ , and  $h$  for the  $(-1, 0)$  resonance. The results are presented in Table 2, and representative fits are shown in Figure 6. The damping parameters are the fwhm of the imaginary part of the dielectric function, which has a Lorentzian shape. The corresponding lifetimes,  $1/(2\pi\gamma c)$ , where  $c$  is the speed of light in vacuum, have been plotted in Figure 7 against the wavelength associated with the fitted transition frequency,  $\nu_i$  (not the peak centers). The fitted curve in Figure 7 gives the lifetime in femtoseconds as  $6.6(13)e^{0.173(9)\lambda}$ , where  $\lambda$  is in micrometers and the uncertainties are given in parentheses. Interestingly, the curve seems to predict lifetimes in the visible that are not far from the ones measured by Dogariuet et al.<sup>59</sup> Lifetimes have been obtained that may be 100 times longer than those in the visible. A resonance with a 510-fs lifetime can travel about 0.150 mm, which is a rather macroscopic distance. This distance is much larger than the  $5\text{-}\mu\text{m}$  thickness of the film,

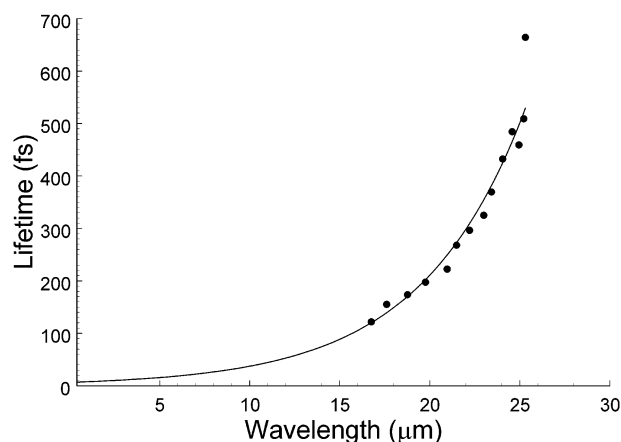


**Figure 7.** Damping constants ( $\gamma$ ) from Table 2 have been converted to lifetimes and are plotted vs the wavelength of the fitted transition frequencies ( $\nu_i$ , not peak centers). In general, the longer wavelengths show longer lifetimes. The lifetimes were fit to an exponential function (solid line) giving a lifetime in femtoseconds of  $6.6e^{0.173\lambda}$ , where  $\lambda$  is in micrometers. The plot extends on the left to the blue edge of the visible range ( $0.400\ \mu\text{m}$ ) to show the agreement of the fitted curve from this work with lifetimes measured in the visible range.

and we wonder whether the resonance condition involves SPPs tunneling back and forth through the hole.

**Stacking.** The stack of two clamped and stretched pieces of Buckbee-Mears Ni mesh shows the same transmission resonances as a single piece, but there appears to be less of the classical diffraction background. (Light initially incident on holes rather than metal can be transmitted, producing a classical diffraction pattern of the array of sources.) The most prominent resonance in Figure 3 shows 60% transmission that is  $\sim 6$  times greater than the fractional open area! The primary resonance breaks into three peaks above  $10^\circ$  just as it does using a single piece of mesh, so the dispersion behavior is that of SPPs. When four pieces of mesh were stacked, we were still able to obtain 22% transmission at the primary resonance, a little of the  $(1, 1)$ ,  $(2, 0)$ , and  $(2, 1)$  resonances, and a flat baseline close to zero elsewhere. The procedure of stacking meshes accentuates the SPP behavior at the expense of the classical diffraction. Clearly, light is being forced to “run” along the metallic surface in the form of SPPs as straight-through transmission is diminished to the point of insignificance. This technique has the potential to vastly extend the effective path length of absorption experiments directed at species on the surface of the metal. It would be useful if the primary resonance could be engineered (by

changing  $L$ ) to be near the strong vibrations of surface molecular species. In general, this requires making meshes with smaller lattice parameters than are currently available commercially from Buckbee-Mears.

**IR Absorption Spectra of a 1-Dodecanethiol Monolayer on Nickel.** The absorption spectra of Figure 4 reveal characteristic absorptions<sup>60,61,65–69</sup> in the C–H stretching region associated with the methylene and methyl groups of the dodecane hydrocarbon chains. The largest peak is assigned to the asymmetric methylene stretch, and the second largest is assigned to a symmetric methylene stretch. These absorptions decay over the course of  $\sim 30$  min, as has previously been seen to occur with alkanethiols on nickel.<sup>70</sup> Remarkably, the initial absolute absorbance of  $\sim 0.11$  for the asymmetric methylene C–H stretch is more than 100 times greater than the absorbances typically seen with reflection absorption infrared spectroscopy (RAIRS), which are  $\sim 0.001$ .<sup>60,67–69</sup> A monolayer coating is absorbing 22% of the light resonant with its most intense vibration! Clearly, there is a great enhancement in absorption due to the unusual optical properties of the array of subwavelength metal apertures. Unfortunately, the finest Buckbee-Mears mesh is available only in Ni, whereas such coatings are stable on Cu or Au.

## Discussion

Surface plasmons have been accessed with mid-IR light on Ni microarrays of subwavelength apertures using zeroth-order FTIR transmission spectra. Because nickel does not show this behavior in the visible, it is somewhat unusual to be able to access SPs on nickel with such a simple approach.

The transmission on the prominent resonance is high enough relative to the fractional open area that it must involve coupling light through the microchannels that is not directly incident upon the hole. The single Buckbee-Mears Ni mesh shows 77% transmission with only a 26% open area; the double-stacked mesh shows 60% transmission with only a 10% open area; and the quadruple-stacked mesh shows 22% transmission with an estimated 0.5% open area. In this sequence, the enhancement of transmitted light over the fractional open area increases from 3 to 6 to  $\sim 40$ , respectively. Light is being guided along the surface of the metal rather than having to impinge upon a hole. There is a small broad background of transmission due to the pattern of apertures that would likely occur even if the apertures were not made of metal. Stacking of the mesh suppresses the “nonmetallic” diffraction background, better isolating the SP behavior.

The narrower resonances observed in the infrared have made fitting with a damped harmonic oscillator model feasible. We have observed resonant lifetimes in the range of 80–510 fs for the  $(-1, 0)$  resonance, which is the most isolated from the rest. These lifetimes are considerably longer than the value of  $\sim 3$  fs that we estimate from the hwhm of Ebbesen’s free-standing silver microarray<sup>35</sup> (resonance at 800 nm) or the 7 fs measured with fast laser pulses.<sup>59</sup> The lifetimes exhibit a smooth exponential dependence with wavelength that should enable investigations of the SP destruction mechanisms. When the lifetimes are considered with photon surface velocities, we obtain distances that are many times greater than the thickness of the mesh. It would be interesting to devise experiments sensitive to the possibility of etalon-like multipassing by matching molecular vibrations of surface-adsorbed species to different resonances of different lifetimes.

The subwavelength metal microarray approach has the potential to change the path length of absorption for surface

species from about twice the thickness of the membrane or coating (as it is in RAIRS, reflection absorption infrared spectroscopy) to the length of the microchannel plus whatever distances the SPs run along the front or back surfaces. We have in fact observed a 100-fold increase in the vibrational absorption of a 1-dodecanethiolate self-assembled monolayer on the Ni mesh. Greater enhancements, narrow resonances, and stable monolayers have been observed when the apertures are closed down by electrodepositing copper onto the Ni mesh, and these will serve as the next subject in this investigation. The subwavelength metal microarray approach will work on a number of other metals, including Pd, Cr, Pt, W, and perhaps semiconductors. This opens SP lines of investigation to a whole new set of chemically interesting metals.

**Acknowledgment.** We thank the donors of the American Chemical Society Petroleum Research Fund (38502-AC5) and The Ohio State University Department of Chemistry for support.

## References and Notes

- (1) Liebsch, A. *Electronic Excitations at Metal Surfaces*; Plenum Press: New York, 1997.
- (2) Andersen, P. C.; Rowlen, K. L. *Appl. Spectrosc.* **2002**, *56*, 124A.
- (3) *Near-Field Optics and Surface Plasmon Polaritons*; Kawata, S., Ed.; Topics in Applied Physics; Springer, Berlin, 2001; Vol. 81.
- (4) *Surface Plasmon-Polaritons*, Proceedings of a One-Day Workshop of the Thin Films and Surfaces Group of the Institute of Physics, London, Nov 25, 1987; Institute of Physics (Great Britain), Thin Films and Surfaces Group: Bristol, England, 1988.
- (5) Raether, H. *Surface Plasmons on Smooth and Rough Surfaces and on Gratings*; Springer-Verlag: Berlin, 1988.
- (6) Smolyaninov, I. I.; Zayats, A. V.; Stanishevsky, A.; Davis, C. C. *Phys. Rev. B* **2002**, *66*, 205414.
- (7) Fukui, M.; So, V. C. Y.; Normandin, R. *Phys. Status Solidi B* **1979**, *91*, K61.
- (8) Homola, J.; Koudela, I.; Yee, S. S. *Sens. Actuators, B* **1999**, *54*, 16.
- (9) Caide, X.; Sui, S.-F. *Sens. Actuators, B* **2000**, *66*, 174.
- (10) Tien, H. T.; Ottova, A. L. *Electrochim. Acta* **1998**, *43*, 3587.
- (11) Salamon, Z.; Wang, Y.; Tollin, G.; Macleod, H. A. *Biochim. Biophys. Acta* **1994**, *1195*, 267.
- (12) Salamon, Z.; Macleod, H. A.; Tollin, G. *Biophys. J.* **1997**, *73*, 2791.
- (13) Salamon, Z.; Huang, D.; Cramer, W. A.; Tollin, G. *Biophys. J.* **1998**, *75*, 1874.
- (14) Salamon, Z.; Cowell, S.; Varga, E.; Yamamura, H. I.; Hruby, V. J.; Tollin, G. *Biophys. J.* **2000**, *79*, 2463.
- (15) Salamon, Z.; Wang, Y.; Brown, M. F.; Macleod, H. A.; Tollin, G. *Biochemistry* **1994**, *33*, 13706.
- (16) Frutos, A. G.; Weibel, S. C.; Corn, R. M. *Anal. Chem.* **1999**, *71*, 3935.
- (17) Nelson, B. P.; Frutos, A. G.; Brockman, J. M.; Corn, R. M. *Anal. Chem.* **1999**, *71*, 3928.
- (18) Faegerstam, L. G.; O’Shannessy, D. J. *Chromatogr. Sci. Ser.* **1993**, *63*, 229.
- (19) Szabo, A.; Stolz, L.; Granzow, R. *Curr. Opin. Struct. Biol.* **1995**, *5*, 699.
- (20) Maystre, D. *Selected Papers on Diffraction Gratings*; SPIE Optical Engineering Press: Bellingham, WA, 1993.
- (21) Wood, R. W. *Philos. Mag.* **1902**, *4*, 396.
- (22) Rayleigh, L. *Philos. Mag. Ser. 6* **1907**, *14*, 60.
- (23) Teng, Y.-Y.; Stern, E. *Phys. Rev. Lett.* **1967**, *19*, 511.
- (24) Ritchie, R. H.; Arakawa, E. T.; Cowan, J. J.; Hamm, R. N. *Phys. Rev. Lett.* **1968**, *21*, 1530.
- (25) Otto, A. *Z. Phys.* **1968**, *216*, 398.
- (26) Kretschmann, E.; Raether, H. *Z. Naturforsch.* **1968**, *23*, 2135.
- (27) Bass, M.; Van Stryland, E. W.; Williams, D. R. *Handbook of Optics*, 2nd ed.; McGraw-Hill: New York, 1995.
- (28) Rakic, A. D.; Djuricic, A. B.; Elazar, J. M.; Majewski, M. L. *Appl. Opt.* **1998**, *37*, 5271.
- (29) Ghaemi, H. F.; Thio, T.; Grupp, D. E.; Ebbesen, T. W.; Lezec, H. *J. Phys. Rev. B: Condens. Matter* **1998**, *58*, 6779.
- (30) Ebbesen, T. W.; Lezec, H. J.; Ghaemi, H. F.; Thio, T.; Wolff, P. A. *Nature (London)* **1998**, *391*, 667.
- (31) Thio, T.; Ghaemi, H. F.; Lezec, H. J.; Wolff, P. A.; Ebbesen, T. W. *J. Opt. Soc. Am. B: Opt. Phys.* **1999**, *16*, 1743.
- (32) Grupp, D. E.; Lezec, H. J.; Thio, T.; Ebbesen, T. W. *Adv. Mater.* **1999**, *11*, 860.

- (33) Grupp, D. E.; Lezec, H. J.; Ebbesen, T. W.; Pellerin, K. M.; Thio, T. *Appl. Phys. Lett.* **2000**, *77*, 1569.
- (34) Krishnan, A.; Thio, T.; Kim, T. J.; Lezec, H. J.; Ebbesen, T. W.; Wolff, P. A.; Pendry, J.; Martin-Moreno, L.; Garcia-Vidal, F. J. *Opt. Commun.* **2001**, *200*, 1.
- (35) Martin-Moreno, L.; Garcia-Vidal, F. J.; Lezec, H. J.; Pellerin, K. M.; Thio, T.; Pendry, J. B.; Ebbesen, T. W. *Phys. Rev. Lett.* **2001**, *86*, 1114.
- (36) Krishnan, A.; Thio, T.; Kim, T. J.; Lezec, H. J.; Ebbesen, T. W.; Wolff, P. A.; Pendry, J.; Martin-Moreno, L.; Garcia-Vidal, F. J. *Opt. Commun.* **2001**, *200*, 1.
- (37) Thio, T.; Lezec, H. J.; Ebbesen, T. W.; Pellerin, K. M.; Lewen, G. D.; Nahata, A.; Linke, R. A. *Nanotechnology* **2002**, *13*, 429.
- (38) Fuzi, Y.; Bradberry, G. W.; Sambles, J. R. *J. Mod. Opt.* **1989**, *36*, 1405.
- (39) Yang, F.; Bradberry, G. W.; Sambles, J. R. *Thin Solid Films* **1991**, *196*, 35.
- (40) Jackson, J. D. *Classical Electrodynamics*, 3rd ed.; Wiley: New York, 1999.
- (41) Bethe, H. A. *Phys. Rev.* **1944**, *66*, 163.
- (42) Bouwkamp, C. J. *Philips Res. Rep.* **1950**, *5*, 321.
- (43) Degiron, A.; Lezec, H. J.; Barnes, W. L.; Ebbesen, T. W. *Appl. Phys. Lett.* **2002**, *81*, 4327.
- (44) Moller, K. D.; Sternberg, O.; Grebel, H.; Lalanne, P. *J. Appl. Phys.* **2002**, *91*, 9461.
- (45) Mittra, R.; Chan, C. H.; Cwik, T. *Proc. IEEE* **1988**, *76*, 1593.
- (46) McPhedran, R. C.; Maystre, D. *Appl. Phys.* **1977**, *14*, 1.
- (47) Ulrich, R. *Infrared Phys.* **1967**, *7*, 37.
- (48) Derrick, G. H.; McPhedran, R. C.; Maystre, D.; Neviere, M. *Appl. Phys.* **1979**, *18*, 39.
- (49) Vigoureux, J. M. *Opt. Commun.* **2001**, *198*, 257.
- (50) Treacy, M. M. J. *Phys. Rev. B: Condens. Matter* **2002**, *66*, 195105/1.
- (51) Popov, E.; Neviere, M.; Enoch, S.; Reinisch, R. *Phys. Rev. B: Condens. Matter* **2000**, *62*, 16100.
- (52) Cao, Q.; Lalanne, P. *Phys. Rev. Lett.* **2002**, *88*, 057403/1.
- (53) Schroter, U.; Heitmann, D. *Phys. Rev. B: Condens. Matter* **1998**, *58*, 15419.
- (54) Wannemacher, R. *Opt. Commun.* **2001**, *195*, 107.
- (55) Porto, J. A.; Garcia-Vidal, F. J.; Pendry, J. B. *Phys. Rev. Lett.* **1999**, *83*, 2845.
- (56) Hooper, I. R.; Sambles, J. R. *Phys. Rev. B: Condens. Matter* **2002**, *66*, 205408/1.
- (57) Hooper, I. R.; Sambles, J. R. *Phys. Rev. B: Condens. Matter* **2002**, *65*, 165432/1.
- (58) Altevischer, E.; van Exter, M. P.; Woerdman, J. P. *Nature (London)* **2002**, *418*, 304.
- (59) Dogariu, A.; Thio, T.; Wang, L. J.; Ebbesen, T. W.; Lezec, H. J. *Opt. Lett.* **2001**, *26*, 450.
- (60) Walczak, M. M.; Chung, C. K.; Stole, S. M.; Widrig, C. A.; Porter, M. D. *J. Am. Chem. Soc.* **1991**, *113*, 2370.
- (61) Laibinis, P. E.; Whitesides, G. M.; Allara, D. L.; Tao, Y. T.; Parikh, A. N.; Nuzzo, R. G. *J. Am. Chem. Soc.* **1991**, *113*, 7152.
- (62) Darmanyan, S. A.; Zayats, A. V. *Phys. Rev. B: Condens. Matter* **2003**, *67*, 035424.
- (63) Barnes, W. L.; Preist, T. W.; Kitson, S. C.; Sambles, J. R. *Phys. Rev. B: Condens. Matter* **1996**, *54*, 6227.
- (64) Decius, J. C.; Hexter, R. M. *Molecular Vibrations in Crystals*; McGraw-Hill: New York, 1977.
- (65) Hou, Z. Z.; Abbott, N. L.; Stroeve, P. *Langmuir* **1998**, *14*, 3287.
- (66) Bensebaa, F.; Ellis, T. H.; Badia, A.; Lennox, R. B. *Langmuir* **1998**, *14*, 2361.
- (67) Jennings, G. K.; Munro, J. C.; Yong, T.-H.; Laibinis, P. E. *Langmuir* **1998**, *14*, 6130.
- (68) Noble-Luginbuhl, A. R.; Nuzzo, R. G. *Langmuir* **2001**, *17*, 3937.
- (69) Ron, H.; Cohen, H.; Matlis, S.; Rappaport, M.; Rubinstein, I. *J. Phys. Chem. B* **1998**, *102*, 9861.
- (70) Mekhalif, Z.; Riga, J.; Pireaux, J. J.; Delhalle, J. *Langmuir* **1997**, *13*, 2285.